Chinese Chemical Letters 35 (2024) 109242

Contents lists available at ScienceDirect

Chinese Chemical Letters

journal homepage: www.elsevier.com/locate/cclet

Manganese oxide and derivative-modified materials in advanced oxidation processes: A review of modification enhancement and activation mechanisms

Si Sun[a,b], Shuang Song[c], Shuai Yang[a,b], Yong-Li He[a,b], Yang Shi[a], Peng Zhou[a,b], Zhao-kun Xiong[a,b], Yang Liu[a,b], Heng Zhang[a,b], Ye Du[a,b], Chuan-Shu He[a,b,*], Bo Lai[a,b]

[a] State Key Laboratory of Hydraulics and Mountain River Engineering, College of Architecture and Environment, Sichuan University, Chengdu 610065, China
[b] Sino-German Centre for Water and Health Research, Sichuan University, Chengdu 610065, China
[c] Institute of Fundamental and Frontier Sciences, University of Electronic Science and Technology of China, Sichuan, Chengdu 610054, China

ARTICLE INFO

Article history:
Received 11 August 2023
Revised 24 October 2023
Accepted 24 October 2023
Available online 29 October 2023

Keywords:
Manganese oxide
Derivative-modified materials
Modification enhancement mechanisms
Advanced oxidation process
Activation mechanism

ABSTRACT

Manganese oxides (MnO_x), as low-toxicity and high-abundance catalysts, have been demonstrated to hold great promise for application in advanced oxidation processes (AOPs). However, further application of this material is restricted due to its unsatisfactory oxidant activation efficiency. Fortunately, recently remarkable research on deep activation mechanisms and modification of MnO_x have been undertaken to improve its reactivity. Herein, modification enhancement mechanisms of MnO_x to efficiently degrade various organic contaminants were discussed and highlighted, including metal doping, coupling with other metal oxides, composite with carbonaceous material, and compounding with other support. The activation mechanisms of different MnO_x and derivative-modified material (such as doped MnO_x, metal oxide-MnO_x hybrids, and MnO_x-carbonaceous material hybrids) were summarized in great details, which was specifically categorized into both radical and non-radical pathways. The effects of pH, inorganic ions, and natural organic matter on degradation reactions are also discussed. Finally, future research directions and perspectives are presented to provide a clear interpretation on the MnO_x initiated AOPs.

1. Introduction

As industrial has civilization advanced, environmental problems have erupted on a large scale, adversely affecting sustainable development [1]. Surface water and groundwater are contaminated to varying degrees, deteriorating water quality [2,3]. Considerable effort has been devoted to developing various technologies for aqueous decontamination [4,5].

In the field of wastewater treatment, AOPs have great potential as they can oxidize various pollutants to harmless compounds [6,7]. It has been demonstrated that highly reactive oxygen species (ROS) (such as $SO_4^{\bullet-}$, $HO^{\bullet}$, $RO^{\bullet}$, $O_2^{\bullet-}$, $IO_3^{\bullet}$, and $^1O_2$) could be efficiently generated from various types of oxidants, such as peroxymonosulfate (PMS), hydrogen peroxide (H_2O_2), peroxydisulfate (PDS), peracetic acid (PAA), ferrate (Fe(VI)), and periodate (PI) in AOPs [8–11]. The redox potential of ROS is higher than that of their parent compounds, making it easier for them to rapidly degrade multiple pollutants [1]. Although activation processes requiring additional energy inputs, such as thermal [12], microwave [13], ultrasonic [14], and illumination [15], they provide enhanced perform with increased energy consumption and costs. Heterogeneous and homogeneous catalysis, by contrast, has the advantages of low energy requirements, easy scale-up and high reactivity [16,17]. Transition-metal ions (such as Mn^{2+}, Cu^{2+}, and Co^{2+}) with perfect catalytic effects, natural abundance and low operating costs are considered a dynamic class of activators. For instance, a homogeneous Co(II)/PAA activation system was established to produce $CH_3COOO^{\bullet}$, which degraded phenol rapidly *via* hydrogen atom abstraction (HAA) [18]. However, secondary pollution caused by the introduction of metal ions has limited further applications of homogeneous catalysis using metal ions [19]. Therefore, it is imperative to develop heterogeneous catalysts.

It was observed that Co-based, Cu-based, Ag-based, and Ru-based catalysts were extensively studied in AOPs [20–22]. However, high costs discourage the use of Ag- and Ru-based catalysts for water treatment. The leaching of toxic metal ions is an Achilles heel for Co- and Cu-based catalysts during environmental remediation applications. Manganese oxide (MnO_x) has abundant reserves in

* Corresponding author.
E-mail address: hecs@scu.edu.cn (C.-S. He).

https://doi.org/10.1016/j.cclet.2023.109242
1001-8417/

nature, low toxicity, and is widely used in the fields of energy and catalysis, as a promising substitute for other metal oxides [23,24]. Moreover, MnO_x is closely related to life. MnO_x minerals in soil are the major source of Mn for plants and directly affect plant growth. Living organisms generally contain low levels of Mn. MnO_x is an important adsorption carrier for some heavy-metal ions, and this property aids in controlling the concentration and distribution of heavy metals in soil and water [25]. In addition, MnO_x affects the fate of organic matter transformations, particularly those of humic substances [26]. Recently, research on MnO_x has expanded to AOPs because of its abundant reserves, low cost, high tunability of catalytic activity, and low toxicity [27,28]. Different phase structures, Mn oxidation states, morphologies, and surface properties are major factors affecting MnO_x reactivity, which were the key components included in these studies [29,30]. The effect of MnO_2 phase structure on the oxidative reactivity has been researched [24]. Mn(III) is a key factor influencing catalytic activity. In addition, deep activation mechanisms in AOPs with MnO_x have also been increasingly studied. In a recent study, organic radicals generated using Mn species cycling were found to be responsible for the degradation of sulfamethoxazole (SMX) in Mn_3O_4/system [31]. In the non-radical pathway, Mn_2O_3 acts as an electron shuttle between PMS and phenol to form long-lived surface-reactive Mn(IV) species, dominating the organic pollutants removal [28]. To better understand the nature of MnO_x and synthesize more desirable low-cost, high-activity, and environmentally friendly catalysts, it is necessary to summarize the results obtained from all the reported studies on use of MnO_x for AOPs. However, the oxidant activation efficiency of pure MnO_x tends to be less than ideal, and the primary reactive species/pathways of pollutant degradation in various AOPs remain controversial. Hence, it is worth focusing on modifying MnO_x to obtain new and effective catalysts, as well as deeper probing into degradation mechanisms. The Mn(III) (oxyhydr) oxides used for activating persulfate (PS) are summarized in a review [32]. This review discussed the crystal structure of manganese(III) (oxyhydr) oxides as well as the effect of catalyst composition and structure on the activation mechanism [32]. Furthermore, Fe-Mn binary oxide, spinel $MnFe_2O_4$, and their applications have been reviewed in the field of water treatment, including adsorption, oxidation, and AOPs [33,34]. The catalysts mentioned above are a class of manganese oxides or their derivatives. They targeted parts of the AOPs that they belonged to a smaller branch. Some other studies have summarized the reported advances in Mn-based catalysts in AOPs [2,25]. A previous review summarized the formation of MnO_x and outlined the application and mechanism by that MnO_x activating various peroxides, which including H_2O_2, O_3 and PS, to degrade pollutants [25]. The promotional effects of modification on the catalytic activity are also discussed. Another review summarized all the reported advances in Mn-based catalysts for PMS/PDS activation [2]. With the development of research, more oxidants such as PAA and PI have gradually gained weight. Therefore, a comprehensive review of Mn-based catalysts for AOPs is required. In addition, the impacts of modification on the catalyst reactivity and mechanism should be examined in greater depth. Over the past five years, research on MnO_x and derivative-modified materials has grown. A summary of the latest catalyst mechanisms and modifications is lacking.

Therefore, the activation and modification enhancement mechanisms need to be summarized to address the gaps in MnO_x and derivative-modified materials application in AOPs. Herein, a comprehensive summary of MnO_x and derivative-modified materials used in AOPs is presented. First, basic synthesis methods for MnO_x are briefly introduced. Subsequently, the relationship between modification and catalyst reactivity, as well as the deep mechanism, were meticulously categorized, discussed, and highlighted. Moreover, the mechanisms of MnO_x and derivative-modified materials were split into radical-dominant and non-radical-dominant. Important factors influencing the reaction process are also elaborated. Finally, the conclusions and future perspectives are presented.

2. Synthesis methods

Previous studies have demonstrated high catalytic activity of manganese oxides owing to their multivalent phase structure, valences and morphologies [32]. Meanwhile, the MnO_x and derivative-modified materials synthesized by different synthesis methods possessed different phase structure and average valence states, leading to the different physicochemical and structural properties, which have an impact on the catalytic activity. Hence, selecting the appropriate synthesis method to obtain the ideal catalyst matters a lot. A summary based on previous studies displayed that hydrothermal [35], sol-gel [36], solvothermal [37], biosynthesis [38] impregnation [39], coprecipitation [40], reflux [41], and calcination [42] are the typical synthetic methods for MnO_x and derivative-modified materials. Various synthesis methods for MnO_x are listed in Table S1 (Supporting information), and those for the derivative-modified materials are listed in Table S2 to Table S4 (Supporting information). The oxidants, contaminants, reactivities, and mechanisms are also involved in Table S1 to Table S4. An overview of the synthesis methods for pure MnO_x, doped MnO_x, metal oxide-MnO_x hybrids, and MnO_x-carbonaceous material hybrids is provided in Texts S1-S4 (Supporting information).

In summary, different synthesis methods yield different materials. The elemental ratio, temperature, reaction time, and solvent polarity are critical factors affecting the morphology, structure, and physicochemical properties of MnO_x and its derivative-modified materials. Therefore, in order to understand the activation mechanisms of MnO_x and derivative-modified materials, it is important to understand the synthesis of MnO_x and derivative-modified materials.

3. Modification enhancement mechanisms

MnO_x is considered as an exceptionally promising candidate catalyst for AOPs, owing to its low cost, high abundance, and environmental friendliness [43]. However, MnO_x reactivity is poor in AOPs; therefore, it is necessary to study the enhancement mechanism of MnO_x and derivative-modified materials.

3.1. Pure MnO_x

3.1.1. Pure MnO_2 and other MnO_x

Manganese dioxide (MnO_2), with various crystalline phases containing α, β, γ, δ, and λ-MnO_2 [44], was affected by different properties resulting in different reactivity. Previous studies have shown that α-MnO_2 possess higher reactivity than that of β-MnO_2 and λ-MnO_2, manifesting crystalline phase is the key factor affecting reactivity. Different crystalline phases have different oxygen liabilities, tunnel sizes, and MnO_6 edges [23], which are the roots cause of their different reactivities. In addition, the content of Mn in different valence states on the surface has been reported to play a leading role in the reactivity. For example, α-MnO_2 was the most active while δ-MnO_2 was the least active, whose activity depended on the Mn(III) content [45]. Furthermore, a higher percentage of Mn(IV) can form Mn(III) faster by reacting with bisulfite (BS), which was attributed to the removal of bisphenol A (BPA) [35]. Moreover, different shapes are related to different surface areas and activities of different facets, which trigger different reactivities. Similar results showed that the reactivity of α-MnO_2 was higher than that of δ-MnO_2 [46], because of higher number of ac-

tive sites and a larger Brunauer Emmett Teller (BET) specific surface area.

Similar to MnO_2, the catalytic reactivity of MnO_x depends on the average oxidation state (AOS), longer bonds between the edge-sharing MnO_6 octahedra, content of surface-OH groups, unique structure, specific surface area and morphology [47]. For instance, the sequence Mn_2O_3 (cubic) > Mn_2O_3 (octahedra) > Mn_2O_3 (truncated) show that different morphologies exhibit different catalytic reactivities [30].

The three factors were summarized to explain the influence of reactivity, namely, (1) Crystalline phase, (2) Intrinsic characteristics including redox potential, AOS, adsorption ability, and conductivity [48], and (3) Surface properties such as surface manganese valence, specific surface area, and morphology.

3.1.2. Pure MnO_x composites

Moreover, various manganese oxide composites have been developed to improve catalyst activity, which featured different morphologies, crystalline phase, surface properties and mixed Mn valence states, such as MnO@MnO_x [49], α-Mn_2O_3@α-MnO_2 [50,51], BioMnO_x [52], Mn_2O_3@Mn_5O_8 [53], and PC-MnO_x (the photochemically synthesized manganese oxides) [54]. For example, α-Mn_2O_3@α-MnO_2 exhibited a higher reactivity than single-phase α-Mn_2O_3 or α-MnO_2, which ascribed to particle size, specific surface area and porosity, potentially efficient mass transfer between core and shell and phase transition from α-MnO_2 to α-Mn_2O_3 [50]. Similar results were obtained for Mn_2O_3@Mn_5O_8 [53] and BioMnO_x [52], whose activity being enhancement was due to the variety of valence states and appropriate particle sizes. Additionally, the oxygen vacancies [49] contributed to the high reactivity, due to the effects of promoting manganese cycling and regulating electronic structure. Therefore, compositing manganese oxide is favorable for adjusting the surface area, AOS, morphology, exposed reactive facets, conductivity, Mn(III), content and oxygen species to enhance our understanding of MnO_x reactivity.

3.1.3. Surface modification

Acidifying MnO_2 and generating oxygen vacancies are effective method for MnO_2 surface modification. The acidified MnO_2 is able to drive phthalate esters (DMP) [55] and polyvinyl alcohol (PVA) [56] degradation. It has been shown that 99% of the DMP was removed within 90 min when the PMS was 1.8 g/L, and 90% of the PVA was degraded by 7 mmol/L PMS in 40 min [55,56]. The surface of acidified MnO_2 (such as MnO_2H-OMS-2 and H2-OMS-2) were equipped with the rich Lewis-acid sites and Brønsted-acid sites, which is conducive to C-C cleavage [55,56]. This was beneficial for the degradation of organic pollutants. In addition, the formation of OVs on the surface of MnO_2 was beneficial to para-chloroaniline (PCA) removal [57].

3.2. Doped MnO_x

First, surface property modification, comprising the addition of active sites and growth in specific surface area, contributes significantly to catalyst reactivity enhancement. Doped MnO_x would introduce other metal sites on the surface, which were regarded as new active sites, affording more excellent catalytic reactivity by the addition of redox cycles. For instance, a new pair of Ce(III)/Ce(IV) [58] and Co(II)/Co(III) redox cycles [59,60] was introduced by Ce doping and Co doping respectively, offering extra routes to better activate PMS. In addition, elemental doping regulated the original Mn redox cycles. For example, Cu doping leads to a higher Mn(IV)/Mn(III) ratio, which encourages Mn(IV)/Mn(III) redox cycles. This is a good way to boost direct/indirect (Cu-AMO-PMS complex-based) phenol oxidation [61].

Elemental doping not only led to new redox cycles and adjusted the original redox cycles, but also promoted the generation of OVs, which is useful for catalyst structure change and performance improvement [62,63]. For example, OVs on the BiOBr surface can motivate hydroxyl ions to generate Bi^{III}-OH and provide electrons for O_2. This is vital for the degradation of organics [62,64]. For MnO_x doped by Cu, the OVs facilitated the complexation of PMS with surface Mn(IV) and accelerate the formation of $^1O_2$ [65]. Moreover, OVs by Ce doping effectively catalyzed the conversion of PMS to $SO_4^{\bullet-}$ and $HO^{\bullet}$ [58]. Therefore, VOs are considered crucial active sites that provide superior catalytic activity for AOPs. Moreover, surface reactive oxygen species favor oxidant activation, which is also considered a valid active site. For example, doping Cu and Nd in OMS-2 favored the formation of abundant surface hydroxyl groups, which stimulated the adsorption of pollutants and the generation of $^1O_2$ [66]. Similar results were shown for MnO_2 doped Ce [67]. It can also be inferred that the changes in the valence that resulted in excellent catalytic performance after doping from the larger specific surface area, which provided more exposed active sites, such as Fe_3O_4/Co-Mn_3O_4 [59].

Second, elemental doping favors interfacial electron transfer and increases the electronic conductivity owing to the redistribution of charge between atoms. For example, the results of electrochemical experiments uncovered that the catalyst with Ce doping has higher current density (Fig. 1a) and greater reductive capability (Fig. 1b) because of the charge transfer capability improved, which is conductive to activate PMS generating $SO_4^{\bullet-}$ and $HO^{\bullet}$ through electron transfer process in Ce-Mn_2O_3/PMS system (Fig. 1c) [58].

3.3. Metal oxide-MnO_x hybrids

3.3.1. Composite with Fe oxides

The magnetic property is a great advantage for catalyst recycling, as the MnO_x catalyst coupled with Fe oxides can be easily recovered under an external magnetic field [68]. It was revealed that the saturation magnetizations of hybrid catalysts, such as MnO_2/$ZnFe_2O_4$ [68], CuS/Fe_2O_3/Mn_2O_3 [69], Fe_3O_4@OMS-2 [70] and Fe_3O_4/MnO_2 [71], were lower than those of the original Fe oxides, but they were strong enough to efficiently separate with the assistance of an external magnetic field. The increase in the application potential arose from the addition of magnetic properties to the catalyst mentioned above. Moreover, the tendency of iron oxides to agglomerate determined their unsatisfactory surface reactivity and consequently limited the removal efficiency, which could be improved by loading MnO_x, which dispersed Fe oxides uniformly to amplify the catalyst reactivity [69].

In addition to their magnetic properties and uniform dispersion, the incorporated Fe oxides influenced reactivity of the catalyst. First, the introduction of Fe oxides provides additional metal active sites to generate ROS more efficiently, similar to the interaction between the doped elements and MnO_x.

Second, the presence of iron oxides leads to synergy between Fe/Mn oxides in the AOPs. Regeneration of active Mn species is greatly accelerated through the reaction between iron and manganese species (Fig. 2a) [72,73]. On the other hand, products of Fe oxides, such as $SO_3^{\bullet-}$, enhanced the production of active Mn species and pollutant degradation, which could also be another kind of synergy between Fe and Mn [74]. The specific impact of the synergistic effect on this mechanism was clarified.

Finally, the combination of Fe oxides and MnO_x can cause changes on the surface of the catalyst. According to previous studies, changes in the specific surface area favorably affect the adsorption and activation processes [75], which could provide more active sites to accelerate the reaction. For example, a higher specific surface area and larger pore volume of the FeMn@K (FeO_x/MnO_y)-modified kaolinite catalyst) than that of bare $MnFe_2O_4$ results in

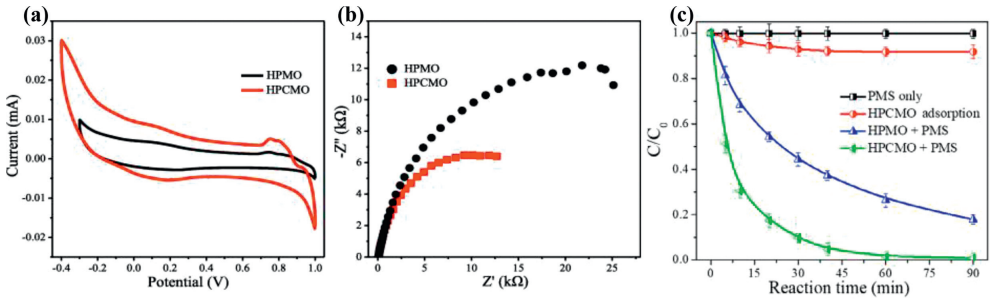

Fig. 1. (a) Cyclic voltammetry plots of HPMO (without Ce doping) and HPCMO (with Ce doping), (b) Nyquist plots of HPMO and HPCMO, and (c) the removal of 2,4-DCP by PMS activation over HPMO and HPCMO. Reprinted with permission [58]. Copyright 2019, Elsevier.

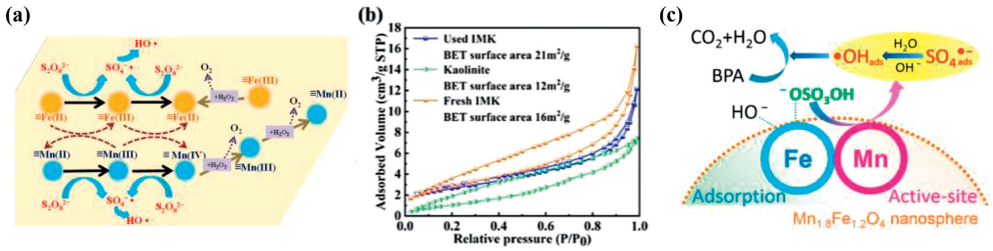

Fig. 2. (a) Regeneration of various metal valence states mechanism in the $F_{4.5}M_1BO$/PS/HP system. Reprinted with permission [73]. Copyright 2019, Elsevier. (b) Nitrogen isotherm adsorption-desorption curves of kaolinite, fresh FeMn@K and used FeMn@K. Reprinted with permission [39]. Copyright 2022, Elsevier. (c) The mechanism that Fe(III) served as adsorption site for the reaction substrates. Reprinted with permission [79]. Copyright 2017, American Chemical Society.

stronger catalytic reactivity for PMS activation and better PVA removal efficiency (Fig. 2b) [39]. A similar result was obtained, where the specific surface area of $CuFe_2O_4$@OMS-2 was 288 m^2/g, which was much larger than those of OMS-2 and $CuFe_2O_4$, with specific surface areas of 129 m^2/g and 7.7 m^2/g [76]. Besides, OVs on the surface were took into consideration to be the active sites, producing $O_2^{\bullet-}$ and $^1O_2$, and enhance the interfacial electron transfer [77]. For example, the OVs on the surface of α-MnO_2/$MnFe_2O_4$, reacted with HSO_5^- to produce $O_2^{\bullet-}$, which was the major ROS and precursor of $^1O_2$ [78]. It also promoted the production of $^1O_2$ by transforming it into active oxygen. And the consumption of OVs was not only involved in the generation process of $O_2^{\bullet-}$ and $^1O_2$, but also used to change the surface loaded hydroxyl (M-OH), which is capable to combine with PMS easily to initiate fast reaction between them. A similar mechanism of PMS activation by the $Mn_{1.8}Fe_{1.2}O_4$ nanospheres was proposed: the production of hydroxyl groups provided primary adsorption sites and promoted the activation of PMS, which is closely related to Fe(III) (Fig. 2c) [79]. Furthermore, surface-adsorbed species and adsorbed molecular water can activate the combined PS and hydrogen peroxide [73]. In summary, the magnetic properties and promotion of oxidant activation, which embrace the additional active reaction and adsorption sites, synergistic effects, and changes in surface properties, were the key enhancement mechanisms after the composite of Fe oxides.

3.3.2. Composite with Cu oxides

Regarding the doping of Cu oxides, the interaction between Mn and the Cu species accounts for the continuous production of active Mn, contributing to the removal of contaminants. In addition, the increase in active sites, specific surface area, and low valence of Mn also created more favorable conditions for the degradation of contaminants, similar to Fe oxides. For example, $CuFe_2O_4$ interacts with the precursor of amorphous MnO_x, resulting in a proportion of Mn(II) and Mn(III). The specific surface area of the $CuFe_2O_4$@OMS-2 catalyst increased significantly, which improved the reactivity of the hybrid catalyst [76]. Furthermore, the absorb H_2O on the surface of $Mn_xCu_yO_z$/γ-Fe_2O_3 increased by doping Cu oxides. They could transform into reactive sites of M-OH, which promoted the decomposition of ozone and generated $HO^{\bullet}$.

3.3.3. Composite with Co oxides

The enhancement mechanism of Co oxides coupled with MnO_x is similar to that of Fe and Cu oxides. However, Co-Mn spinel oxides exhibit a unique enhancement mechanism compared with pure MnO_x. Previous studies have shown that H_2O_2, as a Lewis base, is prone to adsorption on Lewis acid sites and produces considerable amounts of $HO^{\bullet}$ [80]. Meanwhile, PMS and PAA were stimulated to produce more radical by ≡Co-OH^- and ≡Mn-OH^-, such as $SO_4^{\bullet-}$ [81] and $CH_3COOO^{\bullet}$ [19]. These hydroxy forms originate from the reaction between the Lewis acid sites and desorbed H_2O molecules. Compared with single metal oxide catalysts (Co_3O_4 and Mn_2O_3), Co-Mn spinel oxides equipped with more Lewis acid sites can better activate oxidants to produce radicals [80,82]. Moreover, the J-T distortion in a spinel Co doped MnO_x material, produced from the $t_{2g}^3e_g^1$ electronic configuration in Mn sites, breaks the balance of Mn-O in MnO_6 units to accelerate the sustainable performance of PMS activation [81]. Meanwhile, the cooperative effect of Co and Mn atoms not only resulted in the J-T effect but also led to a reduction in the Energy Barrier for PAA Activation and optimization of the distribution of bonding and antibonding states on the Co 3d orbitals [19], which is responsible for superior PAA activation and adsorption properties. In addition, the presence of OVs facilitates the adsorption of reactants and oxidants. The coordination environment and electron spin also determine the catalytic activity of a Co-Mn spinel oxides [83]. In one study, Mn-O has been determined as a catalytically active center. Based on this, the Oh configuration with a stronger orbital overlap between the Mn_{Oh} 3d and O 2p orbitals than the tetrahedron favored Mn-O covalency, thereby accelerating the catalytic reaction. This confirms the positive role of the coordination environment in improving catalytic activity. Regarding the electron spin, Mn doping broke the two extra channels (spin-up and spin-down) for electron transfer between Co_{Oh} and O. This led to a higher activity of Mn than that of Co. Finally, the introduction of Co facilitated the formation of the redox cycles Co(II)/Co(III), Mn(II)/Mn(III), and Co(II)/Mn(III), which

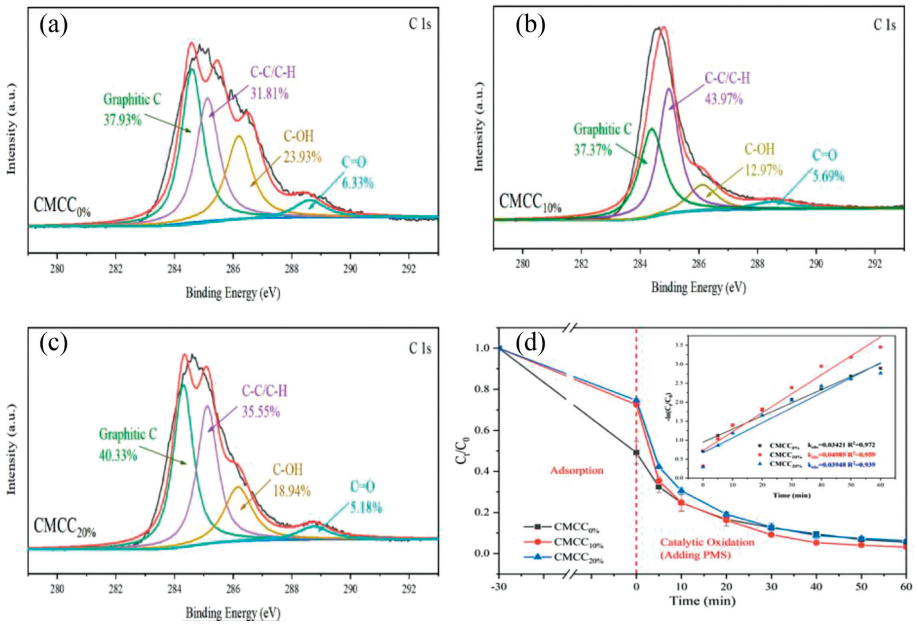

Fig. 3. (a-c) XPS analysis of C 1s for $CMCC_X$ with different percentages (0%, 10%, and 20%) of chitosan. (d) Degradation of BPA by different $CMCC_X$/PMS system. Reprinted with permission [94]. Copyright 2022, Elsevier.

in turn facilitated PMS activation. In general, the increase in the number of Lewis acid sites and redox cycles, introduction of additional electronic states, generation of OVs, and changes in the coordination environment and electron spin have all been considered together facilitated catalyst reactivity.

3.3.4. Polymetallic oxides

Composite of polymetallic oxides and MnO_x exhibiting the sustainable and efficient performance in AOPs, was got more and more attention, such as Bio-$FeMnCoO_x$ [84], $LiNi_{0.5}Co_{0.2}Mn_{0.3}O_2$ [85], Co_3MnFeO_6 [36], MFO-LIBs [86] and Ce-Mn-Co ternary mixed oxide [87]. The superior performance in organic contaminant degradation was ascribed to the presence of more active sites with the introduction of more metals. For example, the major ROS $SO_4^{\bullet-}$ produced in large quantities depended on the synergistic effects between Co, Mn and Fe in Co_3MnFeO_6 catalyst [36]. Fe facilitated the adsorption of CBZ and PMS as well as adding magnetism, and Mn and Co played an irreplaceable role in activating PMS through the redox cycles of Mn(II)/Mn(III), Mn(III)/Mn(IV), and Co(II)/Co(III).

3.4. MnO_x-carbonaceous material hybrids

In addition, MnO_x-carbonaceous material hybrids have also worked efficiently for pollutant degradation in AOPs, such as FeMn@CN-800 in peroxymonosulfate systems [88], Fe/Mn-BC in peroxydisulfate systems [89] and MnO_2-graphite electrodes in the electro-Fenton process [90]. MnO_x-carbonaceous material hybrids could offer more active sites than pure MnO_x, such as ketonic carbonyl groups (C=O), C−C/C−H and zigzag edges on the surface of carbon materials, which was related to higher reactivity of catalysts in AOPs [91–94]. As shown in Fig. 3, $CMCC_X$ with different levels of C−C/C−H led to the different degradation of BPA in PMS activation. This indicated that C–C/C–H can provide active sites. In addition, the introduction of carbon materials can prevent MnO_x aggregation [93] and increase the surface area, which is conducive for exposing more active sites and degrading and accumulating organic pollutants.

The adsorption role of carbon materials has become increasingly important. The carbon matrix provided adsorption sites, lowering the adsorption energy barrier of the pollutant and oxidant, and providing more opportunities for the reaction. For instance, the OMC matrix in MnO_x@OMC strengthened adsorption capacity of catalyst to enrich phenol molecules on the catalytic surface *via* $\pi-\pi$ interaction [95], heightening the likelihood that phenol would react with more $SO_4^{\bullet-}$ and then resulting in the strengthening of catalytic performance [96]. Notably, defects and functional groups in carbon materials play key roles in promoting the adsorption of pollutants and oxidants [97]. It has been shown that abundant defect sites of the carbon-based co-catalyst on $Cu_yMn_{5-y}O_x$/hG promoted the adsorption of PDS and tetracycline (TC) to intensify non-radical processes. TC degraded 99% in 30 min. The different defect levels (Fig. 4) are correlated with the catalytic activity of the catalysts [98].

Furthermore, the carbon matrix can improve the electron transfer efficiency, which is beneficial for degradation mediated by the electron transfer pathway and the interfacial electron transfer process between the catalysts and oxidants. For example, oxidant potential for Mn(III)/Mn(IV) of MnO_x@OMC (0.336 V) was lower than MnO_x (0.455 V), manifesting that the overpotential for $Mn(IV)_{(s)}$ formation declined due to OMC matrix, accelerating interface electron transfer process to produce $SO_4^{\bullet-}$ [96]. Finally, the introduction of carbon materials can change the properties of the MnO_x component in the hybrids in favor of catalyst reactivity. The abundance of low-valent Mn species has been reported to increase since OMS-2 was coupled with g-C_3N_4 and carbon nanofibers (CNFs) [99]. In summary, the addition of active sites, enhancement of the adsorption capacity, improvement of the electron transfer efficiency, and changes in the properties of MnO_x are the advantages of compositing MnO_x with carbonaceous materials. The modification enhancement mechanisms of MnO_x-other support material hybrids are presented in Text S5 (Supporting information).

4. Activation mechanisms of AOPs

4.1. Pure MnO_x

MnO_2, which has a high oxidizing performance and low biotoxicity [100], is considered a promising heterogeneous catalyst for the removal of organic contaminants from AOPs. Generally, $SO_4^{\bullet-}$ and $HO^{\bullet}$ were major reactive oxygen species (ROS) in MnO_2/PS

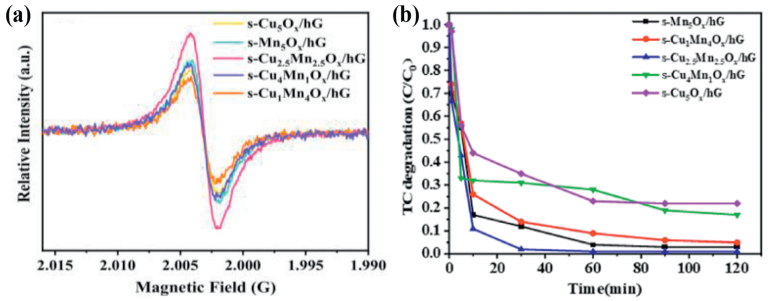

Fig. 4. (a) EPR spectra of defects in different catalysts, and (b) TC removals by PDS activation over different catalysts. Reprinted with permission [98]. Copyright 2022, Elsevier.

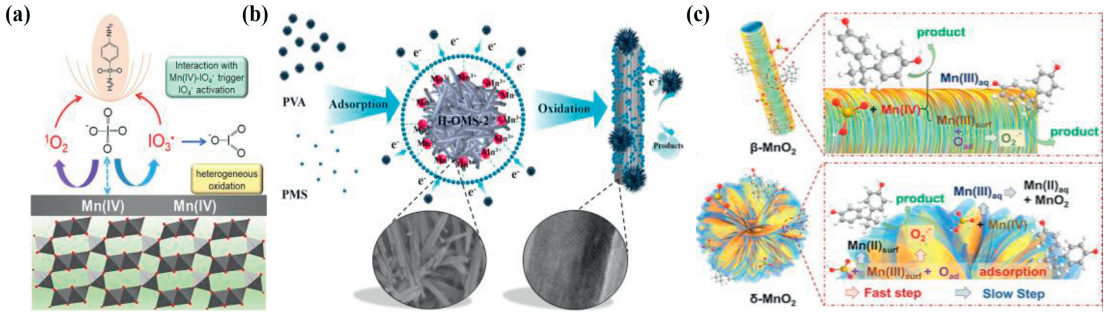

Fig. 5. (a) The plausible PI activation mechanism over MnO_2. Reprinted with permission [110]. Copyright 2020, Elsevier. (b) The proposed PVA oxidation mechanism by direct electron transfer process. Reprinted with permission [56]. Copyright 2022, Elsevier. (c) Dual-path oxidation of BPA triggered by the β-MnO_2/BS system. Reprinted with permission [35]. Copyright 2022, American Chemical Society.

system. The Mn(II) and Mn(III) on the surfaces of MnO_2 as active sites activated PS to generate $SO_4^{\bullet-}$ and $HO^{\bullet}$ in MnO_2/PS system (Eqs. 1–4 for PMS activation, Eq. 5 for PDS activation) [46,101-106]. And then, Mn(III) and Mn(IV), underwent a reduction reaction with PS, returning to low-valence state as well as obtaining $SO_5^{\bullet-}$ and $S_2O_8^{\bullet-}$(Eqs. 6–8). Therefore, the redox cycling Mn(II)/Mn(III) and Mn(III)/Mn(IV) are the key to the production of $SO_4^{\bullet-}$ and $HO^{\bullet}$ in PS activation. Based on persulfate-based AOPs, electro-Fenton processes [107] and photo–Fenton processes [108] were also found to be dominated by $SO_4^{\bullet-}$ and $HO^{\bullet}$. The previous studies shown that the $SO_4^{\bullet-}$ and $HO^{\bullet}$ also were generated by reaction between oxidants (H_2O_2 or $S_2O_8^{2-}$) and low valent manganese (Mn(III) or Mn(II)), and were promoted by the photo-assisted reduction originated from Mn(IV) and the UVA irradiation [109].

As the study progressed, in addition to the radical pathways, non-radical pathways were also shown to be effective for AOPs in the presence of MnO_2. Different phase structures of MnO_2 were chosen to activate PMS, which has been demonstrated that $^1O_2$ formed from $HO^{\bullet}$, facilitated degradation by quenching experiments and electron spin resonance (ESR), as shown in Eq. 9 [45]. Moreover, $^1O_2$ was generated when metastable Mn(IV)-O-IO_3 interacted with sulfanilamide (Fig. 5a) [110].

Additionally, based on PMS decomposition and Raman spectra, the generation of reactive complexes between amorphous MnO_2 and PMS was proposed to mediate the direct electron transfer process (ETP) between the contaminant and PMS to remove the contaminants (Fig. 5b) [56,111].

Furthermore, aqueous $Mn(III)_{aq}$ plays a critical role in the oxidation process because of its high oxidation potential. For example, $Mn(III)_{aq}$ generated by the colloidal MnO_2/HSO_3^- [112] and β-MnO_2/HSO_3^- [35] process degrades EOCs and BPA rapidly (Fig. 5c).

To summarize the reported research, the mechanisms of AOPs presenting MnO_2 can be classified into two types: (1) Radical pathways; $SO_4^{\bullet-}$ and $HO^{\bullet}$ is the primary active species. (2) Non-radical pathways, which primarily include the $^1O_2$ oxidation process, $Mn(III)_{aq}$ oxidation process, and ETP.

$$\equiv Mn(II) + HSO_5^- \rightarrow \equiv Mn(III) + SO_4^{2-} + HO^{\bullet} \quad (1)$$

$$\equiv Mn(III) + HSO_5^- \rightarrow \equiv Mn(IV) + SO_4^{2-} + HO^{\bullet} \quad (2)$$

$$\equiv Mn(II) + HSO_5^- \rightarrow \equiv Mn(III) + SO_4^{\bullet-} + OH^- \quad (3)$$

$$\equiv Mn(III) + HSO_5^- \rightarrow \equiv Mn(IV) + SO_4^{\bullet-} + OH^- \quad (4)$$

$$S_2O_8^{2-} + \equiv Mn(III) \rightarrow SO_4^{\bullet-} + SO_4^{2-} + \equiv Mn(IV) \quad (5)$$

$$\equiv Mn(III) + HSO_5^- \rightarrow \equiv Mn(II) + SO_5^{\bullet-} + H^+ \quad (6)$$

$$\equiv Mn(IV) + HSO_5^- \rightarrow \equiv Mn(III) + SO_5^{\bullet-} + H^+ \quad (7)$$

$$S_2O_8^{2-} + \equiv Mn(IV) \rightarrow S_2O_8^{\bullet-} + \equiv Mn(III) \quad (8)$$

$$4HO^{\bullet} \rightarrow {}^1O_2 + 2H_2O \quad (9)$$

In addition to MnO_2, manganese oxides in different valence states, such as MnO, Mn_2O_3, Mn_3O_4 and MnOOH, have also been used in AOPs [106,113-116]. $SO_4^{\bullet-}$, $HO^{\bullet}$ and $RO^{\bullet}$, acted as primary active species, were primarily generated by the redox cycles of Mn(II)/Mn(III) or Mn(III)/Mn(IV) (Eqs. 10 and 11, similar to MnO_2, are not listed) [31,117-119]. In contrast to the radical pathways, $^1O_2$ was produced by direct oxidation or recombination of $O_2^{\bullet-}$, which

was generated *via* the decomposition of PS facilitated through electron transfer of the Mn species (Eqs. 12–16) [47]. $^1O_2$ could also be capable of removing ciprofloxacin (CIP) by supporting with $SO_4^{\bullet-}$ and $HO^{\bullet}$, revealing the $SO_4^{\bullet-}$, $HO^{\bullet}$ and $^1O_2$ could be existed simultaneously [120]. Additionally, mechanism of the Mn_2O_3 catalyzing PMS activation process was explained that Mn_2O_3 acts as a shuttle, mediating the electron transfer from organic contaminants to PMS (Eqs. 17–19) [28].

$$\equiv Mn(II)/\equiv Mn(III) + CH_3C(O)OOH \rightarrow \equiv Mn(III)/Mn(IV) + CH_3C(O)O^{\bullet} + OH^- \quad (10)$$

$$\equiv Mn(III)/\equiv Mn(IV) + CH_3C(O)OOH \rightarrow \equiv Mn(II)/Mn(III) + CH_3C(O)O^{\bullet} + H^+ \quad (11)$$

$$2\equiv Mn(III/IV)-OH + HS_2O_8^- \rightarrow 2\equiv Mn(III/IV)-OS_2O_7^- + 3H^+ \quad (12)$$

$$2\equiv Mn(III/IV)-OS_2O_7^- + 4H_2O + OS_2O_7^- \rightarrow 2\equiv Mn(III)-OH + 2SO_4^{2-} + O_2^{\bullet-} + HO_2^{\bullet} + 7H^+ \quad (13)$$

$$O_2^{\bullet-} + HO_2^{\bullet} \rightarrow {}^1O_2 + HO_2^- \quad (14)$$

$$O_2^{\bullet-} + HO^{\bullet} \rightarrow {}^1O_2 + HO^- \quad (15)$$

$$2O_2^{\bullet-} + 2H^+ \rightarrow H_2O_2 + {}^1O_2 \quad (16)$$

$$\equiv Mn(III)-OH + HOOSO_3^- \rightarrow \equiv Mn(III)-HOOSO_3^- + H_2O \quad (17)$$

$$\equiv Mn(III)-OOSO_3^- + \equiv Mn(III)-OH \rightarrow \equiv Mn(III)-OO-Mn(III) + SO_4^{2-} + H^+ \quad (18)$$

$$Mn(III)-OO-Mn(III) + 2H_2O \rightarrow 2\equiv Mn(IV)-OH + 2HO^- \quad (19)$$

Studies on various pure manganese oxide composites (*e.g.*, α-Mn_2O_3@α-MnO_2) were summarized. It suggested that Mn(II)/≡Mn(III) on the catalyst crystal surface activated the adsorbed PMS, leading to the generation of $SO_4^{\bullet-}$ and $HO^{\bullet}$. These processes can be accelerated by photogenerated e^- and photolysis [49]. In addition among the widely researched radical mechanisms, $^1O_2$ has also been reported to be imperative in PMS/MnO_x composite systems, in compliance with a self-decomposition and energy quenching mechanism (Eq. 20) [52].

$$HSO_5^- + SO_5^{2-} \rightarrow HSO_4^- + SO_4^{2-} + {}^1O_2 \quad (20)$$

4.2. Doped MnO_x

Elemental doping has been applied to modify MnO_x [121–123], which can be used to readily modulate the electronic structure of MnO_x, boost the mobility of charge carriers, create more active sites, and optimize the kinetics and energetics of catalytic reactions [124]. As a result, it has been regarded as an effective approach for improving catalyst reactivity. It has been reported that Mo-doping can catalyze the N_2 reduction reaction (NRR) in neutral media more robustly than MnO_2 without Mo doping [125]. Doped MnO_x has also been confirmed to be applicable in AOPs [61].

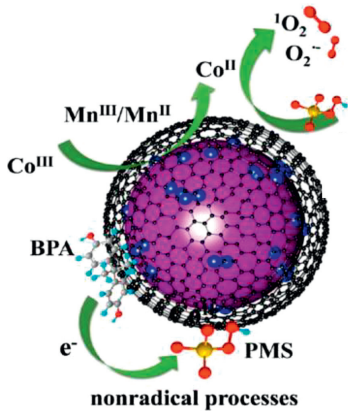

Fig. 6. BPA degradation mechanism by $^1O_2$, $O_2^{\bullet-}$ and ETP in (Co/MnO-0.32@C)/PMS system. Reprinted with permission [126]. Copyright 2022, Elsevier.

4.2.1. Ce doping

The incorporation of 7% Ce doped into MnO_2 enhanced the PMS activation to produce $SO_4^{\bullet-}$ and $HO^{\bullet}$, *via* the strong electronic interaction between Ce and Mn [67], which carried degradation efficiency of TC to a new and higher level. Similarly, the introduction of Ce endows Mn_2O_3 with exceptional PMS activation capabilities. And $SO_4^{\bullet-}$, $HO^{\bullet}$ and $^1O_2$ were detected in Ce-Mn_2O_3/PMS system to degrade 2,4-dichlorophenol (2,4-DCP) [58], instead of only $^1O_2$ involved in Mn_2O_3/PMS system. The value of k_{obs} and TOF are 0.0668 min^{-1} and 0.334 min^{-1} for Ce doped Mn_2O_3, respectively. However, owing to the collapse of the structure, cerium overloading adversely affected PMS activation.

4.2.2. Co doping

Because the Co-Mn synergistic effect improves the catalytic reactivity, Co was chosen as another important dopant. Specifically, Co has been incorporated into MnO [126] and magnetic Mn_3O_4 [59] to degrade organic contaminants with strengthened activity and stability, both of that were dominated by $O_2^{\bullet-}$ and $^1O_2$ and involved radical and non-radical processes (Fig. 6). It has been observed that the redox cycles between metal elements are at the core of radical generation, similar to MnO_2 [127]. And the formation of $^1O_2$ relied heavily on the conversion of $SO_5^{\bullet-}$ and $O_2^{\bullet-}$ (Eqs. 21 and 22) originating from radicals (such as $HO^{\bullet}$ and $HO_2^{\bullet}$) and reactions of HSO_5^- at high-valent metal sites. Moreover, Co-doped biogenic MnO_x [127] was prepared to hasten PMS activation to degrade TC, the mechanism of which is similar to that of the cobalt oxide-MnO_x hybrids elaborated in the following paragraphs.

$$4SO_5^{\bullet-} + 2H_2O \rightarrow 3{}^1O_2 + 4HSO_4^- \quad (21)$$

$$2O_2^{\bullet-} + 2H_2O \rightarrow {}^1O_2 + H_2O_2 + 2OH^- \quad (22)$$

4.2.3. Cu doping

Furthermore, there is a growing body of research on MnO_x doped with Cu [65,128-130], which is dominated by non-radical pathways. $^1O_2$ can be generated because surface oxygen defects can lower the reaction energy barrier of PMS decomposition *via* energy trapping by oxygen (Eqs. 23–25) in a Cu–MnO_2/PMS system [130]. It is as opposed to PMS self-decomposition and the contribution of reaction between $O_2^{\bullet-}$ and $HO^{\bullet}$, which has been frequently reported. Besides, $^1O_2$ could also be formed *via* thermodynamically favored directly oxidation of $O_2^{\bullet-}$ in another Cu-MnO_2/PMS system [65], which was arose from the reaction between metastable intermediates MnIV–O–O–SO_3/Cu^{II}–O–O–SO_3 and PMS.

$$\equiv O_2 \rightarrow O_{ads} \text{ (active site)} \quad (23)$$

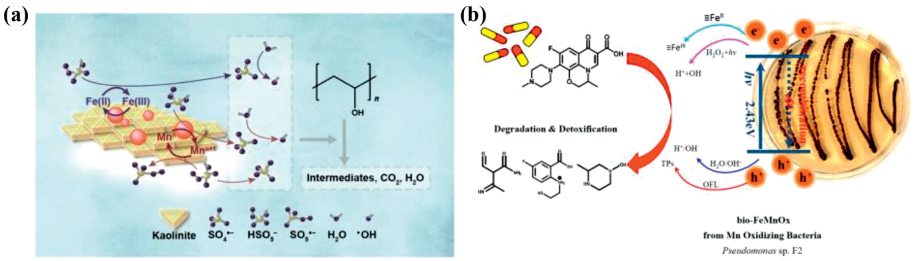

Fig. 7. (a) Possible activation mechanisms of PMS in FeMn@K/PMS system. Reprinted with permission [39]. Copyright 2022, Elsevier. (b) Activation mechanisms of photo-Fenton. Reprinted with permission [136]. Copyright 2020, Elsevier.

$$O_{ads} + PMS \rightarrow \text{decrease energy barrier} \quad (24)$$

$$\equiv O_2 \rightarrow {}^1O_2 \quad (25)$$

Moreover, Co doping became a development trend in MnO_x, such as Cu with Nd [66] and Ce with Co [60], which have a kindred-like mechanism with the single-element doping of MnO_x.

4.3. Metal oxide-MnOx hybrids

Considerable reported research has strongly revealed that synergistic effect between two different metal ions could strengthen catalytic activity of catalysts. Therefore, metal oxide-MnO_x hybrids synthesized by metal oxides coupling with MnO_x have been used in AOPs, such as MnO_2/NiO [131], Fe_3O_4/α-MnO_2 [132] and α-MnO_2@CuO membrane [133]. In addition, various bimetallic oxides-MnO_x hybrid oxides and polymetallic oxides-MnO_x hybrid oxides have been investigated, exhibiting superior catalytic performance and stability for pollutant removal, such as $MnFe_2O_4$ [134,135], bio-FeMnO_x [136], Co_3MnFeO_6 [36], and $LiNi_{0.5}Co_{0.2}Mn_{0.3}O_2$ [85].

4.3.1. Fe oxides

Among these, Fe oxides have been widely studied because of their magnetic properties, high abundance, and low toxicity [137]. Magnetite (Fe_3O_4), Fe_2O_3, and $CuFe_2O_4$ were composited with MnO_x and Fe-Mn binary oxides (FMBOs) were synthesized to efficiently produce ROS. The release of $SO_4^{\bullet-}$ and HO$^\bullet$ was generated by ≡Mn(II)/≡Mn(III) and ≡Fe(II)/≡Fe(III) complexing with HSO_5^- and $S_2O_8^{2-}$ on the surface of the catalyst (Eqs. 26–29), such as CuS/Fe_2O_3/Mn_2O_3 [69], FMBOs [72], FeO_x/MnO_y (Fig. 7a) [39], Fe_3O_4-MnO_2 [138], Fe_3O_4-α-MnO_2 [132], γ-Fe_2O_3/Mn_3O_4 [139] and α-MnO_2/$MnFe_2O_4$ [78]. Additionally, $SO_4^{\bullet-}$ was also generated through the catalytic process of Fe_2O_3/$NaHSO_3$ in Fe-Mn_X/BS system with energy input [74]. Similarly, HO$^\bullet$ was also formed in the photo-Fenton system in presence of bio−FeMnO_x (Eq. 30 and Fig. 7b) [136].

However, it has been demonstrated that Fe(III)/Fe(II) has a lower catalytic activity than Mn(III)/Mn(II) (1.54 eV) and Mn(IV)/Mn(II) (1.69 eV) because of its lower redox potential (0.77 eV) [140,141]. In addition to providing additional reactive sites, Fe oxides play a role in accelerating the recycling of Mn species and the generation of active Mn(III) species, as shown in Eqs. 31–33. These processes were realized by Fe(II) reducing Mn(III/IV) and $SO_3^{\bullet-}$ (the products of Fe(III) oxidizing HSO_3^-) reducing Mn(IV), respectively. For example, Fe(II) could reduce Mn(III) and Mn(IV), allowing the continuous formation of $SO_5^{\bullet-}$ and $SO_4^{\bullet-}$ in FeO_x/MnO_y combined PMS system [39] and α-MnO_2/$MnFe_2O_4$ combined PMS system [78]. And $SO_3^{\bullet-}$ promoted the formation of Mn(III) was present in Fe-MnX/BS system, both of that contributed to the removal of methylene blue (MB) dye.

$^1O_2$ was also ROS in MFBOs system [142] and α-MnO_2/$MnFe_2O_4$ system [78], which primarily came from the self-decomposition of PMS (Eq. 20), transformation from OVs to active oxygen (Eqs. 34 and 35), and the reaction of $O_2^{\bullet-}$ (Eqs. 14–16).

$$\equiv Fe(III) + HSO_5^- \rightarrow \equiv Fe(II) + SO_5^{\bullet-} + H^+ \quad (26)$$

$$\equiv Fe(II) + HSO_5^- \rightarrow \equiv Fe(III) + SO_4^{\bullet-} + OH^- \quad (27)$$

$$S_2O_8^{2-} + Fe(II) \rightarrow SO_4^{\bullet-} + Fe(III) + SO_4^{2-} \quad (28)$$

$$Fe(III) + H_2O \rightarrow Fe(III) + HO^\bullet + H^+ \quad (29)$$

$$\equiv Fe(III) + H_2O/OH^- \xrightarrow{hv} OH^\bullet + H^+ + e_{cb}^- \quad (30)$$

$$Mn(III) + Fe(II) \rightarrow Mn(II) + Fe(III), \quad E^0 = 0.204\ V \quad (31)$$

$$Mn(IV) + 2Fe(II) \rightarrow Mn(II) + 2Fe(III), \quad E^0 = 0.714\ V \quad (32)$$

$$SO_3^{\bullet-} + Mn(IV) + 2OH^- \rightarrow Mn(III) + H_2O + SO_4^{2-} \quad (33)$$

$$OVs \rightarrow \text{active oxygen} \quad (34)$$

$$\text{active oxygen} + HSO_5^- \rightarrow HSO_4^- + {}^1O_2 \quad (35)$$

4.3.2. Cu oxides

Cu oxides are more catalytically active compared than their homogeneous counterparts. Therefore, Cu oxides are excellent candidates for fabricating composites with MnO_x. In the presence of Cu oxide-MnO_x hybrids, $SO_4^{\bullet-}$ and HO$^\bullet$ was produced more than in the presence of pure MnO_x or pure Cu oxides. It depended on the dual redox cycles of Mn(III)/Mn(IV) and Cu(I)/Cu(II), which means that incorporation of Cu created more active sites to react with oxidant, such as Mn_3O_4/$CuBi_2O_4$ [143], α-MnO_2@CuO [133] and CuO@OMS-2 [144] in PMS activation. And HO$^\bullet$ could also be generated by the reaction between ozone and surface hydroxyl group, transformed from the absorb H_2O on the surface of $Mn_xCu_yO_z$/γ-Fe_2O_3 in catalytic ozonation (Eq. 36).

Moreover, the Cu species are involved in accelerating the conversion of Mn species with different valence states. For example, the Cu species in $CuFe_2O_4$@OMS-2 [76] hardly participated directly in PMS activation but could reduce Mn species with a high oxidation state, generating more active Mn species for PMS activation. However, the reaction that HSO_5^- ($E_{(HSO_5^-/HSO_4^-)} = 1.8$ V) reduced Cu(II) ($E_{(Cu(II)/Cu(I)} = 0.15$ V) is thermodynamically unfavorable, leading to the transformation from Cu(II) to a higher valence copper (Eqs. 37–39) have been proposed [145].

$$O_3 + -OH \rightarrow HO^\bullet \quad (36)$$

$$\equiv Cu(II)-OH^- + HSO_5^- \rightarrow \equiv Cu(II)-(HO)OSO_3^-OH^- \quad (37)$$

$$\equiv Cu(III)-OH^- + HSO_5^- \rightarrow \equiv Cu(II)-(HO)OSO_3^- + H_2O \quad (38)$$

$$\equiv Cu(II)-(HO)OSO_3^- \rightarrow \equiv Cu(III)-OH^- + SO_4^{\bullet-} \quad (39)$$

4.3.3. Co oxides

Co oxides were also selected as the group for composition with MnO_x, such as Mn-Co/γ-Al_2O_3 [146], $Mn_xCo_{3-x}O_4$ [147], and MCW (composites embracing Mn, Co, and W) [148], which activate PMS to produce the $SO_4^{\bullet-}$, $HO^{\bullet}$, $O_2^{\bullet-}$ and $^1O_2$. The $SO_4^{\bullet-}$ and $HO^{\bullet}$ was produced from changes in the valence of Mn species, Co species and Mn/Co species. And the $O_2^{\bullet-}$ was originated from O_2, which was transformed from lattice oxygen (Eq. 40). In addition, $^1O_2$ was produced by the self-decomposition of PMS.

$$O_2 + e^- \rightarrow O_2^{\bullet-} \quad (40)$$

Furthermore, multiple valence states and more electron transfer pathways were observed in Co-Mn spinel oxides, which have the potential for application in low-cost and simple fabrication [19,149,150]. Therefore, achieving the targets for efficient pollutant removal from AOPs is highly promising. The generation of $SO_4^{\bullet-}$ and $HO^{\bullet}$ was similar to the bimetallic oxide of cobalt oxide combined with Mn referred above in Co-Mn spinel oxides/PMS system [151].

Moreover, $HO^{\bullet}$ and $O_2^{\bullet-}$ could be generated to display superior sonocatalytic activity in oxytetracycline (OTC) degradation by $MnCo_2O_{4+\sigma}$ under ultrasonic irradiation (Eq. 41) [152]. When it comes to photocatalyst-PMS activation coupling system, $SO_4^{\bullet-}$ was originated from the reaction between PMS and the photogenerated electrons driven to the catalyst surface (Eqs. 42 and 43), the metal-hydroxyl species with low-valent state (≡Co(II)–OH, ≡Mn(II)–OH, and ≡Mn(III)–OH) (Eqs. 44–46) and $HO^{\bullet}$ (Eq. 47) [81]. As for $HO^{\bullet}$, ≡Co and ≡Mn ions reacted with PMS and $SO_4^{\bullet-}$ reacted with OH^- (Eq. 48), which explains their clear formation.

$$O_2/H_2O + MnCo_2O_{4+\delta} \xrightarrow{US} ROS: HO^{\bullet}/H_2O_2,\ O_2^{\bullet-},\ etc. \quad (41)$$

$$CoMnO_x + hv \rightarrow CoMnO_x(e^-) + CoMnO_x(h^+) \quad (42)$$

$$CoMnO_x(e^-) + HSO_5^- \rightarrow SO_4^{\bullet-} + OH^- \quad (43)$$

$$\equiv Co^{II}-OH + HSO_5^- \rightarrow \equiv Co^{III}-OH + SO_4^{\bullet-} + OH^- \quad (44)$$

$$\equiv Mn^{II}-OH + HSO_5^- \rightarrow \equiv Mn^{III}-OH + SO_4^{\bullet-} + OH^- \quad (45)$$

$$\equiv Mn^{III}-OH + HSO_5^- \rightarrow \equiv Mn^{IV}-OH + SO_4^{\bullet-} + OH^- \quad (46)$$

$$HO^{\bullet} + HSO_5^- \rightarrow SO_4^{\bullet-} + OH^- \quad (47)$$

$$OH^- + SO_4^{\bullet-} \rightarrow SO_4^{2-} + HO^{\bullet} \quad (48)$$

The acetylperoxyl radical ($CH_3C(O)OO^{\bullet}$) is the primary ROS that efficiently degrades sulfamethoxazole (SMX) in the $Co_{3-x}Mn_xO_4$/peracetic acid (PAA) system (Fig. 8) [19], stemming from the electron transfer from PAA to the metal-hydroxyl species in a high-valent state (Eqs. 49-51) and the attack from $CH_3C(O)O^{\bullet}$ to PAA (Eq. 52) [19]. And the values of k_{obs} and TOF (turnover frequency) were 0.54 min^{-1} and 21.6 min^{-1} in this system. Moreover, reduction potential of Mn(IV)/Mn(III) (0.15 V) and Mn(III)/Mn(II)

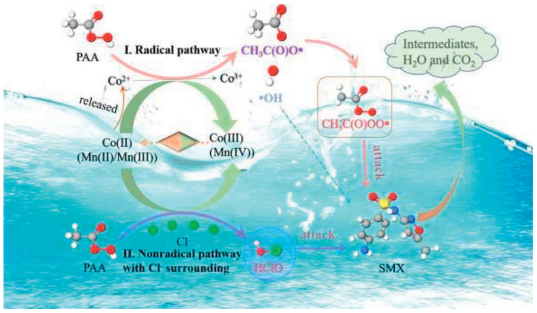

Fig. 8. The proposed PAA activation mechanism to produce RO•. Reprinted with permission [19]. Copyright 2023, Elsevier.

(1.51 V) are lower than Co(III)/Co(II) (1.81 V), which uncovered that Mn(II) and Mn(III) reduced Co(II) to facilitate the redox cycling of Co(III)/Co(II) thermodynamically favorable.

$$\equiv Co(III)-OH^- + CH_3C(O)OOH \rightarrow \equiv Co(II)-OH^- + CH_3C(O)OO^{\bullet} + H^+ \quad (49)$$

$$\equiv Mn(III)-OH^- + CH_3C(O)OOH \rightarrow \equiv Mn(II)-OH^- + CH_3C(O)OO^{\bullet} + H^+ \quad (50)$$

$$\equiv Mn(IV)-OH^- + CH_3C(O)OOH \rightarrow \equiv Mn(III)-OH^- + CH_3C(O)OO^{\bullet} + H^+ \quad (51)$$

$$CH_3C(O)OOH + CH_3C(O)O^{\bullet} \rightarrow CH_3C(O)OO^{\bullet} + CH_3C(O)OH \quad (52)$$

In addition to common Fe, Cu, and Co oxides, oxides of other elements such as Ni [131], Ce [153], Li [154] and Mg [155] have been coupled with MnO_x in various AOPs.

4.4. MnO_x-carbonaceous material hybrids

Recently, carbonaceous materials with tunable electronic and physicochemical features, superior acid and alkali resistances, large surface areas, abundant reserves, and strong biocompatibility have led to the rapid development [1]. In contrast to pure MnO_x, carbonaceous materials compounded with MnO_x have diverse influences on pollutant degradation mechanisms in AOPs in contrast to pure MnO_x.

The production of radicals relies primarily on metal sites in AOPs with MnO_x-carbonaceous, and the increase in radical production is attributed to the redox cycles of different metal species, which is similar to metal oxides alone [98,156-160]. Additionally, radicals, such as $SO_4^{\bullet-}$ and $HO^{\bullet}$, also was available from the reaction at surface oxygen-containing functional groups and the defect structure of the material, produced from the introduction of carbonaceous materials [161]. However, the ratio of non-radical pathways increased with the addition of carbon materials compared to that of pure metal systems.

In addition to the self-decomposition of PMS and superoxide radicals oxidation [37,162], $^1O_2$ was generated at the electron-rich ketonic groups (−C=O) on the surface of carbonaceous materials in AOPs with MnO_x-carbonaceous material, which was considered as an active site to activate PMS, leading to the cleavage of peroxide O−O bond in the PMS [41,163]. For example, the −C=O within CNT (carbon nanotube) was able to catalyze PMS to produce $^1O_2$ [40], and both of −C=O and defects on the surface of mMFC-6 (Mn-Fe oxycarbide) could do the same [163].

Another non-radical pathway, electron transfer, facilitates the oxidation of contaminants through the formation of surface-activated complexes from the adsorption of oxidants on surface

active sites, and transfer from pollution as electron donors to oxidants as electron acceptors mediated by catalysts. For example, surface-activated complexes generated from a combination of surface Mn(III) and PMS boosted electron transfer from the contaminant to Mn-BBC, facilitating the oxidation of the contaminants [38]. Functional groups on carbon materials, such as C−C/C−H, carboxyl and hydroxyl groups [94], could be also active sites for adsorption of PMS to produce metastable PMS.

Radical pathways coexist with non-free radical pathways in many systems [41,164]; for example, both ROS and ETP have been observed to jointly contribute to roxarsone (ROX) decomposition in ball milling multi-walled carbon nanotubes with electrolytic manganese residue (MT/EMR)/PDS systems [165]. Typically, radical-induced oxidation, oxidation by $^1O_2$ and electron transfer-mediated oxidation are the three pathways involved in the presence of $MnFe_2O_4$/MX and PMS. The activation mechanisms of the MnO_x-other support material hybrids are shown in Text S6 (Supporting information).

5. Factors influencing the reactivity

5.1. Effects of pH

The pH has a significant impact on AOPs, which is reflected in the distinct degradation effects of different systems at different pH values. The reasons why the optimal pH values for the different studies varied are explained below.

The classic Fenton reaction usually tends to be confined to acidic environments, and the degradation efficiency is seriously inhibited when pH > 4 [166] because iron precipitates in neutral and alkaline environments, forming iron sludge. Heterogeneous Fenton or Fenton-like processes can extend the applicable pH range to neutral [167]. This is a bottleneck for pollutant removal because of the remarkable decomposition of H_2O_2 above pH 9. For example, as the pH increased from acidic to neutral, the degradation rate of CIP decreased from 69% to 42% during the electro-Fenton process with $MnCo_2O_4$ modifying cathode [168].

In persulfate-based activation systems, degradation rates are usually inhibited under acidic conditions (pH < 3). On the one hand, acidic environments can lead to the dissolution of Mn on the catalyst surface, which in turn may lead to the loss of active sites and alteration of the surface structure of the catalyst [160], ultimately leading to the inhibition of reactivity. In contrast, the competition between protons and catalysts for binding to PS [169] and quenching of the active species by H^+ reduces the activity of the catalyst [170,171]. For example, the degradation rate of CIP slowed owing to the inhibitory effect of H^+ on the generated radicals, resulting in a lower oxidation potential when the pH reached 3 in a system where $CuS/Fe_2O_3/Mn_2O_3$ and PMS existed together [69]. Under alkaline conditions (pH > 10), both improved and inhibited degradation was possible. Enhancement effect was related to the base activation of PMS [172] and the formation of more surface hydroxyl groups (−OH) on the catalyst surface [37], which provided more active sites and species. Dampening effect was originated from suppression of $HO^•$ generation, consumption of PMS (from HSO_5^- to SO_5^{2-}) as well as the self-quenching of $SO_4^{•-}$ [173] respectively.

Most importantly, the electronegativity of the catalyst surface, PS ionization, and pollutant molecules affect the outcome of the degradation reaction [174]. For instance, there were no obvious changes in the degradation efficiency of CBZ in the pH range of 3 to 6.5, but there was a slight decrease at pH 8.0−10 in the Fe_3O_4-MnO_2-ZIF-67/PMS system. This is because when pH > 7, the surface of Fe_3O_4-MnO_2-ZIF-67 is negatively charged owing to the zero point of charge with a value of 6.3, and PMS is primarily in the form of HSO_5^-. Hence, the strong electrostatic repulsion between Fe_3O_4-MnO_2-ZIF-67 and PMS inhibited the degradation effect [156]. In addition, the application of the pH could be broadened by other properties of the contaminants. For example, BPA was adsorbed on the surface of catalyst by π-π and hydrophobic interaction, limiting the effect of the pH [88].

Finally, the pH affects the interconversion of radicals, which in turn affects the degradation of pollutants. The reaction between $SO_4^{•-}$ and HO^- would deplete $SO_4^{•-}$ to produce $HO^•$ when pH > 7 [175,176]. However, the reduction potential of $HO^•$ is lower while the lifetime of $HO^•$ is much shorter (20 ns) compared to $SO_4^{•-}$ (30–40 μs) [177], which might lead to the inhibition of the contaminant degradation at higher pH.

5.2. Water anions

The impact of anions in water on the activation of oxidants is summarized as follows: (1) competing with pollutants by reacting with active species or oxidants, (2) changing the pH, and (3) affecting the adsorption and reaction of pollutants and oxidants on the catalyst surface.

All of carbonate (CO_3^-)/bicarbonate (HCO_3^-), nitrite (NO_2^-)/nitrate (NO_3^-), chloride ion (Cl^-) and dihydrogen phosphate ion ($H_2PO_4^-$) compete with pollutants by reacting with active species or oxidant. It is widely believed that HCO_3^- perceived as a scavenger for highly reactive radicals or oxidants, can react fast with $SO_4^{•-}$, $HO^•$ and IO_4^- to produce less reactive carbonate radicals ($CO_3^{•-}$ and $HCO_3^•$) to hinder degradation of pollutants [78,110]. In contrast, inhibition of pollutant removal is not caused by depletion of active species in PAA activation system [31], owing to previous research uncovered that HCO_3^- is difficult to react with $RO^•$ [178,179]. Hence, it has been proposed that the generation of unreactive Mn complexes inhibits SMX degradation in the PAA system [31]. Besides, HCO_3^- could enhance the reactivity by reacting with PDS to form a oxidant HCO_4^- [180]. The presence of Cl^- exhibits mild inhibition at low concentrations and promotion at high concentrations [102]. The inhibition sprang from the quenching of $SO_4^{•-}$ and $HO^•$ to generate less reactive chlorine radicals and the promotion derived from the formation of active chlorines including $Cl^•$ and HClO [181,182]. HPO_4^{2-}, NO_2^- and NO_3^- can also quench $SO_4^{•-}$ and $HO^•$ to produce $H_2PO_4^•$, $NO_2^•$ and $NO_3^•$ with lower activity thereby inhibiting reactivity [88,183]. Thus, non-radical dominated systems are less disturbed by anions.

Hydrolysis of weak acid anions CO_3^-, HCO_3^- and HPO_4^{2-} leads to a change in the pH of the solution, which is another way for anions in water to influence oxidant activation [155]. For example, with the addition of 3 mmol/L bicarbonate to the solution, the pH of the solution increased to 6.2, which lead to the weakening of PMS activation, by negative charge on the surface of MnO_2 and the increasing repulsion between MnO_2 and HSO_5^- surfaces [108].

Finally, the influence of water anions on the adsorption and reaction of pollutants and oxidants on the catalyst surface was investigated. HPO_4^{2-} deactivates the catalyst surface *via* masking of active sites and competing adsorption sites. For example, HPO_4^{2-} adsorbed and attached to the surface OH groups of CeMO nanocomposites, inhibiting the production of radicals [67]. In addition, HPO_4^{2-} could coordinate with Mn(IV) to compete with PMS, which inhibited PMS adsorption to generate surface-active Mn(IV) [28]. Both pathways strongly influence pollutant degradation.

5.3. Natural organic matter

Natural organic matter (NOM) is widely found in natural waters. It is usually inhibitory to AOPs because of the masking of the active site *versus* the quenching of the active species. For example, fulvic acid (FA) is a NOM. It not only blocked the active sites by

adsorbing onto the surface of Mn_3O_4 but also quenched the active species in this system, leading to the inhibition of SMX degradation [31]. However, NOM can facilitate contaminant removal in a few peroxymonosulfate-based systems owing to the promotion of PMS activation by semiquinone radicals stemming from NOM [184]. Moreover, enhanced pollutant removal was observed in the photocatalytic systems, which was attributed to the fact that NOM can act as a natural photosensitizer [185].

6. Conclusions and perspective

This review focused on the activation mechanism of MnO_x and derivative-modified materials in AOPs, as well as the enhancement mechanism after modification. The analysis of the activation mechanisms involved both radical and non-radical mechanisms. The enhancement mechanism was elaborated for MnO_x, doped MnO_x, metal oxide-MnO_x hybrids, MnO_x-carbonaceous material hybrids, and MnO_x-other support material hybrids. Moreover, it briefly summarized the preparation method for MnO_x and effects of various influencing factors on the degradation reaction, including pH, water anions, and NOM, were investigated. Although many MnO_x-based catalysts with superior performance have been developed, it is essential to recognize that their development in the environmental field has just initiated and faces various challenges. Deep theoretical research and practical applications still have a long way to go and the following issues require further study:

First, there are four outlooks for the mechanistic aspects as follows.

(1) It has been demonstrated that Mn(III) was deemed as an active center of catalytic reaction. However, the role of the Mn species in other valence states is usually overlooked. Specifically, Mn(IV) can be instrumental in PMS adsorption to enable efficient Mn(IV)/Mn(III) operation [186]. Therefore, the functions of various valence states of Mn in MnO_x and derivative-modified materials must be explored in depth.
(2) There has been much more research on PMS activation for organic contaminant degradation than for other oxidants by employing MnO_x and derivative-modified materials. Given that PDS, PAA, O_3 and PI are also considered indispensable oxidants in AOPs and that their activation mechanisms are different from those of PMS, studying the activation mechanisms of other oxidants is important.
(3) More effort should be devoted to theoretical calculations and modeling methods. It is beneficial to understand the different modification effects on MnO_x at the molecular level and explain the changes in the electronic structure and reaction energies of the modifications more clearly.
(4) Some studies have not delved deeply into the activation mechanisms. Therefore, a deeper discussion of the underlying mechanisms is required. The key factors that play a decisive role in the formation of radicals should not be overlooked.

Secondly, two outlooks for modification are listed below.

(1) Metals (Fe, Co, and Cu) are used significantly more in MnO_x modification than in non-metallic doping (N, B, and Se), which could be attributed to the difficulty in successful non-metallic doping. With nonmetallic doping holding promise [187], it is worthwhile to address this difficulty.
(2) Morphology regulation and advanced structure construction can enhance catalyst reactivity through promoting the formation of oxygen vacancies and surface defects, facilitating charge motion, increasing the specific surface area, and boosting mass transportation and light-harvesting [188,189], while different exposed facets have different catalytic activities and adsorption performances. However, few studies have focused on morphology regulation, advanced structure construction, and exposed facets of MnO_x and derivative-modified materials in AOPs. Therefore, there is an urgent need to adjust the morphology to be more conducive to activation, develop more advanced structures (such as ultrathin 2D/2D structures), and controllably synthesize precise and specified exposed facets.

In the final analysis, the activation and enhancement mechanisms of MnO_x and derivative-modified materials are critical for the development of MnO_x-based catalysts for AOPs. We hope that this study will provide guidance for future theoretical research and environmental applications.

Declaration of competing interest

The authors declare that they have no known competing financial interests or personal relationships that could have appeared to influence the work reported in this paper.

Acknowledgments

The authors wish to thank the National Natural Science Foundation of China (Nos. 52170088 and 52070133) for financial support.

Supplementary materials

Supplementary material associated with this article can be found, in the online version, at doi:10.1016/j.cclet.2023.109242.

References

[1] X. Duan, H. Sun, S. Wang, Acc. Chem. Res. 51 (2018) 678–687.
[2] J. Huang, H. Zhang, Environ. Int. 133 (2019) 105141.
[3] M. Afzal, M. Yu, C. Tang, et al., Environ. Int. 129 (2019) 451–460.
[4] Y.Z. Lin, L.B. Zhong, S. Dou, et al., Environ. Int. 128 (2019) 37–45.
[5] C.Y. Chan, H.S. Chan, P.K. Wong, Chemosphere 222 (2019) 371–380.
[6] J. Lin, J. Zou, H. Cai, et al., Water Res. 207 (2021) 117796.
[7] Z. Wang, J. Wang, B. Xiong, et al., Environ. Sci. Technol. 54 (2020) 464–475.
[8] X. Wang, Z. Xiong, H. Shi, et al., Appl. Catal. B 329 (2023) 122569.
[9] R.R. Ding, W.Q. Li, C.S. He, et al., Appl. Catal. B 291 (2021) 120069.
[10] W. Ren, L. Xiong, X. Yuan, et al., Environ. Sci. Technol. 53 (2019) 14595–14603.
[11] S. Yang, Y. Shi, X. Wang, et al., Water Res. 242 (2023) 120317.
[12] G. Wang, P. Wang, H. Liu, et al., Chem. Eng. J. 408 (2021) 127255.
[13] M. Cao, P. Xu, K. Tian, et al., Chem. Eng. J. 471 (2023) 144208.
[14] J. Abdi, A.J. Sisi, M. Hadipoor, et al., J. Hazard. Mater. 424 (2022) 127558.
[15] X.H. Yi, H. Ji, C.C. Wang, et al., Appl. Catal. B 293 (2021) 120229.
[16] L. Wang, J. Jiang, J. Ma, et al., Chem. Eng. J. 427 (2022) 131721.
[17] Z. Wu, Y. Wang, Z. Xiong, et al., Appl. Catal. B 277 (2020) 119136.
[18] P. Du, J. Wang, G. Sun, et al., Water Res. 212 (2022) 118113.
[19] L. Zhang, J. Chen, T. Zheng, et al., Water Res. 229 (2023) 119462.
[20] L. Zhang, J. Chen, Y. Zhang, et al., Water Res. 216 (2022) 118322.
[21] P. Li, Y. Lin, S. Zhao, et al., Appl. Catal. B 298 (2021) 120596.
[22] Y. Zhang, B.T. Zhang, Y. Teng, et al., J. Hazard. Mater. 400 (2020) 123290.
[23] E. Saputra, S. Muhammad, H. Sun, et al., Environ. Sci. Technol. 47 (2013) 5882–5887.
[24] J. Huang, S. Zhong, Y. Dai, et al., Environ. Sci. Technol. 52 (2018) 11309–11318.
[25] S. Zhu, S.H. Ho, C. Jin, et al., Environ. Sci. Nano 7 (2020) 368–396.
[26] H.S.a.P.M. Huang, Nature 298 (1982) 363–365.
[27] K.Z. Huang, H. Zhang, Environ. Sci. Technol. 53 (2019) 12610–12620.
[28] H. Li, N. Yuan, J. Qian, et al., Environ. Sci. Technol. 56 (2022) 4498–4506.
[29] E. Saputra, S. Muhammad, H. Sun, et al., Appl. Catal. B 142-143 (2013) 729–735.
[30] E. Saputra, S. Muhammad, H. Sun, et al., Appl. Catal. B 154-155 (2014) 246–251.
[31] R. Zhou, G. Zhou, Y. Liu, et al., Chemosphere 306 (2022) 135506.
[32] D. Jia, K. Hanna, G. Mailhot, et al., Molecules 26 (2021) 5748.
[33] Y. Chen, Y. Liu, Y. Li, et al., Chem. Eng. J. 388 (2020) 124313.
[34] D. Chu, H. Dong, Y. Li, et al., J. Hazard. Mater. 439 (2022) 129631.
[35] Y. Zhou, X. Li, X. Chen, et al., ACS ES&T Water 2 (2022) 2579–2589.
[36] L. Zhang, X. Zhao, C. Niu, et al., Chem. Eng. J. 362 (2019) 851–864.
[37] Y. Zhao, X. Zhan, H. Wang, et al., Chem. Eng. J. 433 (2022) 133806.
[38] B. Gao, S. Zhu, J. Gu, et al., J. Hazard. Mater. 431 (2022) 128549.
[39] S. Zhai, Y. Chen, Y. Zhu, et al., Appl. Surf. Sci. 605 (2022) 154723.
[40] L. Jin, S. You, X. Duan, et al., J. Hazard. Mater. 423 (2022) 127111.
[41] Y. Wu, Y. Li, J. He, et al., J. Colloid Interface Sci. 562 (2020) 1–11.
[42] K.K. Hazarika, H. Talukdar, P. Sudarsanam, et al., Appl. Organomet. Chem. 34 (2020) e5512.

[43] G. Chen, X. Zhang, Y. Gao, et al., Sep. Purif. Technol. 213 (2019) 456–464.
[44] H. Usui, S. Suzuki, Y. Domi, et al., ACS Sustain. Chem. Eng. 8 (2020) 9165–9173.
[45] J. Huang, Y. Dai, K. Singewald, et al., Chem. Eng. J. 370 (2019) 906–915.
[46] Z.G. Zhou, H.M. Du, Z. Dai, et al., Chem. Eng. J. 374 (2019) 170–180.
[47] A. Khan, K. Zhang, P. Sun, et al., J. Colloid Interface Sci. 584 (2021) 885–899.
[48] J. Zhao, R. Liao, Q. Wang, et al., Sci. Total Environ. 753 (2021) 141835.
[49] A. Wang, Z. Chen, Z. Zheng, et al., Chem. Eng. J. 379 (2020) 122340.
[50] E. Saputra, H. Zhang, Q. Liu, et al., Chemosphere 159 (2016) 351–358.
[51] A. Khan, H. Wang, Y. Liu, et al., J. Mater. Chem. A 6 (2018) 1590–1600.
[52] N. Tian, X. Tian, Y. Nie, et al., Chem. Eng. J. 352 (2018) 469–476.
[53] A. Khan, S. Zou, T. Wang, et al., Phys. Chem. Chem. Phys. 20 (2018) 13909–13919.
[54] S. Zhu, P. Xiao, X. Wang, et al., J. Hazard. Mater. 427 (2022) 127938.
[55] L. Zhang, X. Bi, Z. Wang, et al., Chemosphere 291 (2022) 132740.
[56] N. Yao, H. Zhao, X. Liu, et al., Sep. Purif. Technol. 302 (2022) 122047.
[57] Y. Deng, P. Gao, L. Wang, et al., J. Environ. Chem. Eng. 10 (2022) 107481.
[58] N. Tian, X. Tian, Y. Nie, et al., Chem. Eng. J. 355 (2019) 448–456.
[59] L. He, H. Li, J. Wang, et al., Environ. Sci. Pollut. Res. Int. 29 (2022) 39249–39265.
[60] M.H. Wu, J. Shi, H.P. Deng, Arab. J. Chem. 11 (2018) 924–934.
[61] F. Meerburg, T. Hennebel, L. Vanhaecke, et al., Microb. Biotechnol. 5 (2012) 388–395.
[62] Y. Bu, H. Li, W. Yu, et al., Environ. Sci. Technol. 55 (2021) 2110–2120.
[63] A. Sarkar, G.G. Khan, Nanoscale 11 (2019) 3414–3444.
[64] L. Wu, Z. Sun, Y. Zhen, et al., Environ. Sci. Technol. 55 (2021) 15400–15411.
[65] J. Wang, J. Fan, J. Yao, et al., Chem. Eng. J. 461 (2023) 142024.
[66] X. Wang, X. Bi, N. Yao, et al., Chem. Eng. J. 442 (2022) 136180.
[67] C. Fang, Y. Huang, Y. Wang, et al., J. Water Process. Eng. 50 (2022) 103284.
[68] Y. Wang, H. Sun, H.M. Ang, et al., ACS Appl. Mater. Interfaces 6 (2014) 19914–19923.
[69] Y. Huang, L.c. Nengzi, X. Zhang, et al., Chem. Eng. J. 388 (2020) 124274.
[70] M. Wei, Y. Ruan, S. Luo, et al., New J. Chem. 39 (2015) 6395–6403.
[71] Y.G. Kang, H. Yoon, C.S. Lee, et al., Water Res. 151 (2019) 413–422.
[72] G. Barzegar, M. Sabaghan, O. Azadbakht, et al., Water Sci. Technol. 87 (2023) 1029–1042.
[73] X. Xu, Y. Yang, Y. Jia, et al., Chem. Eng. J. 374 (2019) 776–786.
[74] Z. Hou, J. Ma, C. Fan, et al., Ceram. Int. 45 (2019) 892–898.
[75] X. Xu, R. Lin, X. Deng, et al., Sep. Purif. Technol. 275 (2021) 119184.
[76] P. Ye, D. Wu, M. Wang, et al., Appl. Surf. Sci. 428 (2018) 131–139.
[77] M. Li, Z. He, H. Zhong, et al., Chem. Eng. J. 441 (2022) 136024.
[78] L.S. Xu, X.B. Sun, J.-m. Hong, et al., J. Phys. Chem. Solids 153 (2021) 110029.
[79] G.X. Huang, C.Y. Wang, C.W. Yang, et al., Environ. Sci. Technol. 51 (2017) 12611–12618.
[80] S. Wang, X. Zhang, G. Chen, et al., Chin. Chem. Lett. 33 (2022) 5208–5212.
[81] J. Li, X. Li, X. Wang, et al., Appl. Catal. A: Gen. 584 (2019) 117170.
[82] J. Kim, Y.J. Choe, S.H. Kim, Chem. Eng. J. 413 (2021) 127550.
[83] Z.Y. Guo, C.X. Li, M. Gao, et al., Angew. Chem. Int. Ed. 60 (2020) 274–280.
[84] A. Xu, S. Fan, T. Meng, et al., Appl. Catal. B 318 (2022) 121833.
[85] Y. Zhao, H. Wang, J. Ji, et al., J. Colloid Interface Sci. 626 (2022) 564–580.
[86] J. Liang, M. Guo, Y. Xue, et al., Chem. Eng. J. 435 (2022) 135000.
[87] Q. Wang, W. Deng, X. Lin, et al., J. Rare Earths 39 (2021) 826–834.
[88] F. Hu, Y. Liu, X. Shi, et al., Colloids Surf. A Physicochem. Eng. Asp. 649 (2022) 129520.
[89] K. Zhang, D. Huang, Y. Zhang, et al., J. Environ. Manage. 335 (2023) 117540.
[90] Z.I. Abbas, A.S. Abbas, J. Environ. Chem. Eng. 7 (2019) 103108.
[91] X. Duan, Z. Ao, H. Sun, et al., ACS Appl. Mater. Interfaces 7 (2015) 4169–4178.
[92] X. Duan, S. Indrawirawan, H. Sun, et al., Catal. Today 249 (2015) 184–191.
[93] J. Yu, J. Zhang, T. Zeng, et al., Sep. Purif. Technol. 213 (2019) 264–275.
[94] Z. Wang, Z. Yang, L. Liu, et al., Sep. Purif. Technol. 302 (2022) 122107.
[95] W. Teng, Z. Wu, J. Fan, et al., Energy Environ. Sci. 6 (2013) 2765.
[96] P.C. Guo, H.B. Qiu, C.W. Yang, et al., J. Hazard. Mater. 402 (2021) 123846.
[97] S.M. Shaheen, A.Mosa Natasha, et al., Bioresour. Technol. 346 (2022) 126581.
[98] Y. Sun, R. Xiong, J. Zhang, et al., Sep. Purif. Technol. 293 (2022) 121066.
[99] J. Li, J. Fang, L. Gao, et al., Appl. Surf. Sci. 402 (2017) 352–359.
[100] Y.J. Zhang, J.J. Chen, G.X. Huang, et al., Proc. Natl. Acad. Sci. U. S. A. 120 (2023) e2302407120.
[101] Y. Zhao, Y. Zhao, R. Zhou, et al., RSC Adv. 6 (2016) 35441–35448.
[102] J. Liu, F. An, M. Li, et al., Bull. Environ. Contam. Toxicol. 107 (2021) 255–262.
[103] Y. Xiao, Y. Wang, Y. Xie, et al., Environ. Technol. 41 (2020) 2037–2048.
[104] C. Liu, D. Pan, X. Tang, et al., Water Air Soil Pollut. 227 (2016) 92.
[105] R. Huang, P. Gao, J. Zhu, et al., Appl. Catal. B 317 (2022) 121753.
[106] Y. Li, L.D. Liu, L. Liu, et al., J. Mol. Catal. A: Chem. 411 (2016) 264–271.
[107] L.R. Aveiro, A.G.M. Da Silva, E.G. Candido, et al., Chemosphere 208 (2018) 131–138.
[108] A. Eslami, M. Hashemi, F. Ghanbari, J. Clean. Prod. 195 (2018) 1389–1397.
[109] M. Kamagate, M. Pasturel, M. Brigante, et al., Environ. Sci. Technol. 54 (2020) 476–485.
[110] J. Du, G. Xiao, Y. Xi, et al., Water Res. 169 (2020) 115278.
[111] L. Wang, J. Jiang, S.Y. Pang, et al., Chem. Eng. J. 352 (2018) 1004–1013.
[112] B. Sun, Z. Xiao, H. Dong, et al., J. Hazard. Mater. 363 (2019) 412–420.
[113] M. Liu, M. Lin, P. Wu, et al., Sep. Purif. Technol. 310 (2023) 123052.
[114] R. Shokoohi, M. Salari, A. Shabanloo, et al., Int. J. Environ. Anal. Chem. 102 (2020) 3786–3805.
[115] X. Long, H. Zhang, X. Cao, et al., Sep. Purif. Technol. 303 (2022) 122144.
[116] D. He, Y. Li, C. Lyu, et al., Chemosphere 255 (2020) 126961.
[117] A. Shabanloo, M. Salari, N. Shabanloo, et al., J. Mol. Liq. 298 (2020) 112088.
[118] D. Jia, O. Monfort, K. Hanna, et al., J. Clean. Prod. 328 (2021) 129652.
[119] Q. Wang, Y. Li, Z. Shen, et al., Appl. Surf. Sci. 495 (2019) 143568.
[120] Y. Chi, P. Wang, M. Lin, et al., Chemosphere 299 (2022) 134437.
[121] S. Adjimi, J.M. García-Vargas, J.A. Díaz, et al., Appl. Catal. B 219 (2017) 459–466.
[122] S. Biswas, A.S. Poyraz, Y. Meng, et al., Appl. Catal. B 165 (2015) 731–741.
[123] C.K. King'ondu, N. Opembe, C.-h. Chen, et al., Adv. Funct. Mater. 21 (2011) 312–323.
[124] H. Jin, C. Guo, X. Liu, et al., Chem. Rev. 118 (2018) 6337–6408.
[125] K. Chu, Y.P. Liu, Y.B. Li, et al., Appl. Catal. B 264 (2020) 118525.
[126] Y. Zhao, B. Li, Y. Li, et al., J. Colloid Interface Sci. 623 (2022) 775–786.
[127] H. Luo, Y. Xie, J. Niu, et al., J. Chem. Technol. Biotechnol. 94 (2019) 752–760.
[128] C. Zang, S. Hu, S. Jin, et al., ChemCatChem 10 (2018) 3576–3582.
[129] Y. Yang, P. Zhang, K. Hu, et al., Appl. Catal. B 286 (2021) 119903.
[130] Y. Huang, X. Tian, Y. Nie, et al., J. Hazard. Mater. 360 (2018) 303–310.
[131] X. Zhang, J. Ma, C. Fan, et al., J. Alloys Compd. 785 (2019) 343–349.
[132] Y. Zhao, F. Luo, R. Zhou, Water 14 (2022) 3312.
[133] X. Luo, H. Liang, F. Qu, et al., Chemosphere 200 (2018) 237–247.
[134] F.V. de Andrade, A.B. de Oliveira, G.O. Siqueira, et al., J. Environ. Chem. Eng. 9 (2021) 106232.
[135] J. Liang, R. Chen, J.N. Gu, et al., Water Res. 232 (2023) 119685.
[136] Z. Du, K. Li, S. Zhou, et al., Chem. Eng. J. 380 (2020) 122427.
[137] H. Rashid, P.V. Nidheesh, Catalysts 13 (2023) 195.
[138] J. Liu, Z. Zhao, P. Shao, et al., Chem. Eng. J. 262 (2015) 854–861.
[139] Q. Ma, X. Zhang, R. Guo, et al., Sep. Purif. Technol. 210 (2019) 335–342.
[140] P. Duan, T. Ma, Y. Yue, et al., Environ. Sci. Nano 6 (2019) 1799–1811.
[141] J. Du, J. Bao, Y. Liu, et al., Chem. Eng. J. 376 (2019) 119193.
[142] X. Wang, Y. Xie, K. Chen, et al., Chem. Eng. J. 427 (2022) 130804.
[143] J. Zhang, W. Zhao, S. Wu, et al., J. Hazard. Mater. 410 (2021) 124623.
[144] J. Li, P. Ye, J. Fang, et al., Appl. Surf. Sci. 422 (2017) 754–762.
[145] T. Zhang, H. Zhu, J.P. Croue, Environ. Sci. Technol. 47 (2013) 2784–2791.
[146] Y. Li, Z. Wang, Z. Zou, et al., Sep. Purif. Technol. 302 (2022) 122132.
[147] X. Hu, Y. Ye, Y. Chen, et al., J. Hazard. Mater. 421 (2022) 126841.
[148] X. Luo, Y. You, M. Zhong, et al., J. Hazard. Mater. 426 (2022) 127803.
[149] Y. Peng, H. Tang, B. Yao, et al., Chem. Eng. J. 414 (2021) 128800.
[150] S. Wang, S. Liu, X. Chen, et al., Chem. Eng. J. 453 (2023) 139901.
[151] F. Yang, Y. Lu, X. Dong, et al., J. Hazard. Mater. 424 (2022) 127647.
[152] R. Hassandoost, A. Kotb, Z. Movafagh, et al., Chem. Eng. J. 431 (2022) 133851.
[153] J. Zhou, Y. Sun, W. Sun, et al., Catalysts 12 (2022) 1019.
[154] X. Wang, X. Zhang, L. Dai, et al., ACS Sustain. Chem. Eng. 8 (2020) 11337–11347.
[155] J. Yu, W. Qiu, X. Lin, et al., Chem. Eng. J. 459 (2023) 141574.
[156] L. Dong, Y. Li, X. Chen, et al., Adv. Mater. Interfaces 8 (2021) 2100178.
[157] L. Dong, Y. Li, D. Chen, et al., ACS ES&T Water 1 (2020) 417–429.
[158] H. Fu, S. Ma, P. Zhao, et al., Chem. Eng. J. 360 (2019) 157–170.
[159] K. Wu, C. Tao, M. Wang, et al., Chem. Eng. J. 448 (2022) 137587.
[160] J. Du, J. Bao, Y. Liu, et al., J. Hazard. Mater. 320 (2016) 150–159.
[161] D. Huang, Q. Zhang, C. Zhang, et al., Chem. Eng. J. 391 (2020) 123532.
[162] Y. Wang, Y. Tong, D. Chen, et al., Chem. Eng. J. 459 (2023) 141643.
[163] J.-C.E. Yang, Y. Lin, H.-H. Peng, et al., Appl. Catal. B 268 (2020) 118549.
[164] L. Wang, Q. Jin, Y. Xiang, et al., Chem. Eng. J. 435 (2022) 134877.
[165] M. Li, Z. He, H. Zhong, et al., Water Res. 200 (2021) 117266.
[166] A. Xu, X. Sun, S. Fan, et al., Sep. Purif. Technol. 312 (2023) 123348.
[167] C. Lai, X. Shi, L. Li, et al., Sci. Total Environ. 775 (2021) 145850.
[168] X. Mi, Y. Li, X. Ning, et al., Chem. Eng. J. 358 (2019) 299–309.
[169] Z. Dong, Q. Zhang, B.-Y. Chen, et al., Chem. Eng. J. 357 (2019) 337–347.
[170] Y. Hong, H. Zhou, Z. Xiong, et al., Chem. Eng. J. 391 (2020) 123604.
[171] Q.T. Sun, B.D. Xu, J. Yang, et al., Chem. Eng. J. 400 (2020) 125899.
[172] C. Qi, X. Liu, J. Ma, et al., Chemosphere 151 (2016) 280–288.
[173] M. Feng, R. Qu, X. Zhang, et al., Water Res. 85 (2015) 1–10.
[174] S. Qu, C. Li, X. Sun, et al., Sep. Purif. Technol. 224 (2019) 132–141.
[175] Q. Peng, Y. Ding, L. Zhu, et al., Sep. Purif. Technol. 202 (2018) 307–317.
[176] Q. Ma, H. Zhang, X. Zhang, et al., Chem. Eng. J. 360 (2019) 848–860.
[177] J. Wang, S. Wang, Chem. Eng. J. 334 (2018) 1502–1517.
[178] M. Cai, P. Sun, L. Zhang, et al., Environ. Sci. Technol. 51 (2017) 14217–14224.
[179] P. Xie, J. Ma, W. Liu, et al., Water Res. 69 (2015) 223–233.
[180] M. Jiang, J. Lu, Y. Ji, et al., Water Res. 116 (2017) 324–331.
[181] H. Lin, S. Li, B. Deng, et al., Chem. Eng. J. 364 (2019) 541–551.
[182] H. Zeng, X. Zhao, F. Zhao, et al., Sci. Total Environ. 728 (2020) 138826.
[183] N.S. Shah, J.Ali Khan, M. Sayed, et al., Chem. Eng. J. 356 (2019) 199–209.
[184] Y.H. Guan, J. Ma, Y.M. Ren, et al., Water Res. 47 (2013) 5431–5438.
[185] X. Chen, W. Wang, H. Xiao, et al., Chem. Eng. J. 193-194 (2012) 290–295.
[186] Z.Y. Guo, C.X. Li, M. Gao, et al., Angew. Chem. Int. Ed. 60 (2021) 274–280.
[187] T. He, X. Zeng, S. Rong, J. Mater. Chem. A 8 (2020) 8383–8396.
[188] F. Wang, H. Dai, J. Deng, et al., Environ. Sci. Technol. 46 (2012) 4034–4041.
[189] Y. Li, L. Ji, R. Liu, et al., J. Mater. Chem. A 6 (2018) 12842–12875.